

CONTENTS.

1. Input mode data.
2. Propagation model (reverse).
 - 2.1 Clipping at cold stop.
 - 2.2 Efficiency.
 - 2.3 Rest of instrument.

Summary.

The beam patterns at key components are given for the centre of the longest wavelength channel (0.5mm), TE11 mode only. This is for the purposes of component sizing & stray-light calculation. However, these affects are not assessed in this version as they must await the filling in of the complete picture, in terms of the full set of modes & at the other centre wavelengths (work which is still in progress).

1. Input mode data.

So far, the longest wavelength channel (centre 0.5mm wavelength) has been analysed, in its lowest order mode, i.e. TE11, smooth-walled circular horn. The E-field at the horn aperture is as per fig.1.

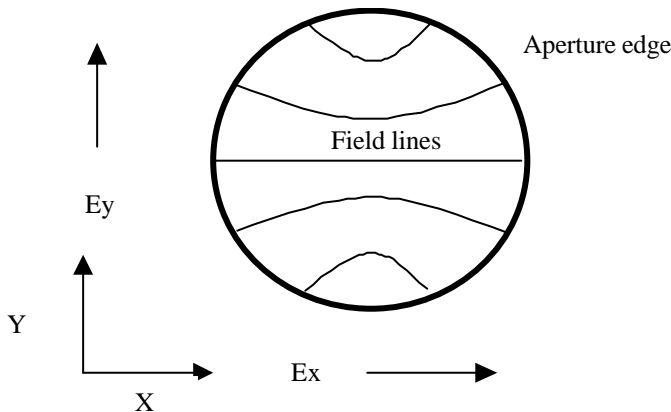


Fig.1a. E-field pattern of mode.

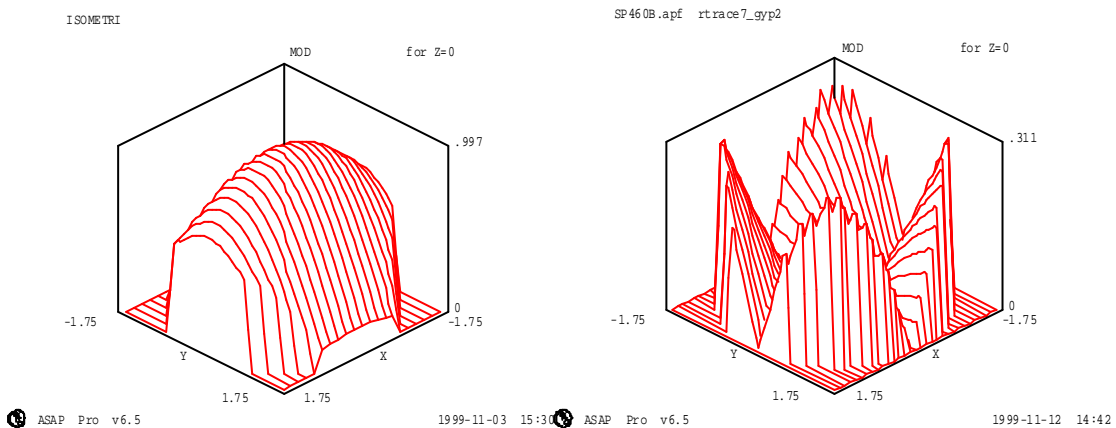


Fig.1b. Input field modulus in cartesian components: Ex (left), Ey (right).

In all beam plots the lateral scale is in millimetres. Thus the horn aperture has 1.75mm radius. NB. The peak Ey field is 30% of the peak Ex.

For propagation the field has to be converted (decomposed) into gaussian modes. Since the pattern is near a focal point and is only a few wavelengths across, this conversion is done as the angular spectrum of plane waves. For maximum resolution the angular range used is that of a full hemisphere (+- 90 degrees), for which the reconstructed pattern is as per fig.2.

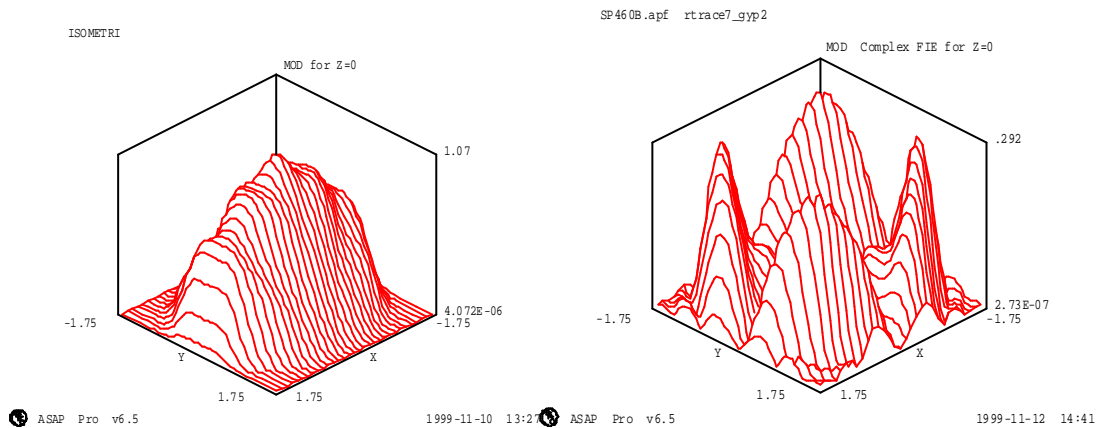


Fig.2a. Best representation in hemisphere angular spectrum ray-set (plots as per fig.1).

Since we aren't really interested in polarisation, it is also useful to look at the total field, i.e. the resultant of the two components, as shown in fig.2b. on the right.

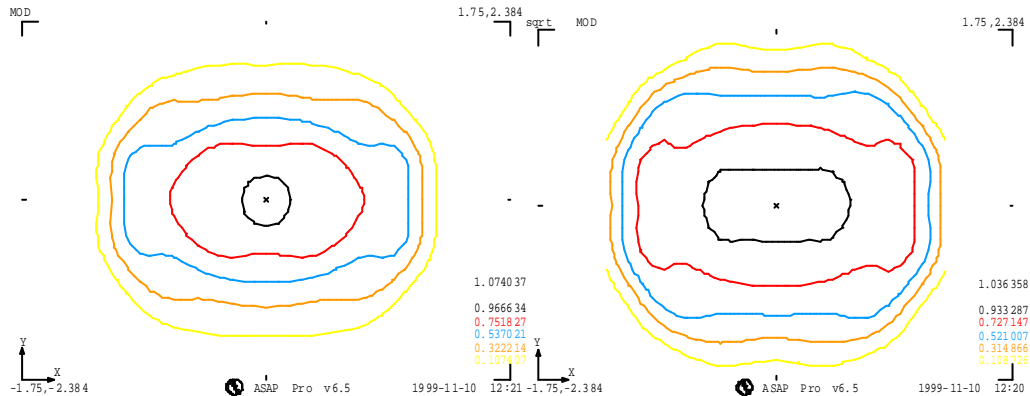


Fig.2b. Contour plot: Left: Ex component only. Right: Total field (resultant of Ex & Ey).

N.B. The contribution of the Ey component makes the total-field beam look more symmetric in shape than it is in the Ex part.

Comparing figures 1 & 2, there are two limitations of the accuracy of the analysis: (1) Distortion of the beam shape towards rectangular features, due to the of cartesian (x-y) sampling. (2) Limited resolution of sharp features i.e. edges. In fig.1. the sample spacing is approx. $\lambda/4$. As this is significantly less than a wavelength, some of the energy is diffracted at angles > 90 degrees, and into non-propagating evanescent

modes. Also, later on the higher spatial frequencies in this pattern (angles > 10 degrees) are filtered out by the clipping action of the cold stop. These effects lead to reduced detection efficiency for the mode, as is discussed later.

2. Propagation model (reverse).

Fig.4 shows the system propagation model. The above input beam is defined at the detector (object #19), with X of the pattern chosen to lie along X of the system, and propagated outwards (time reversed).

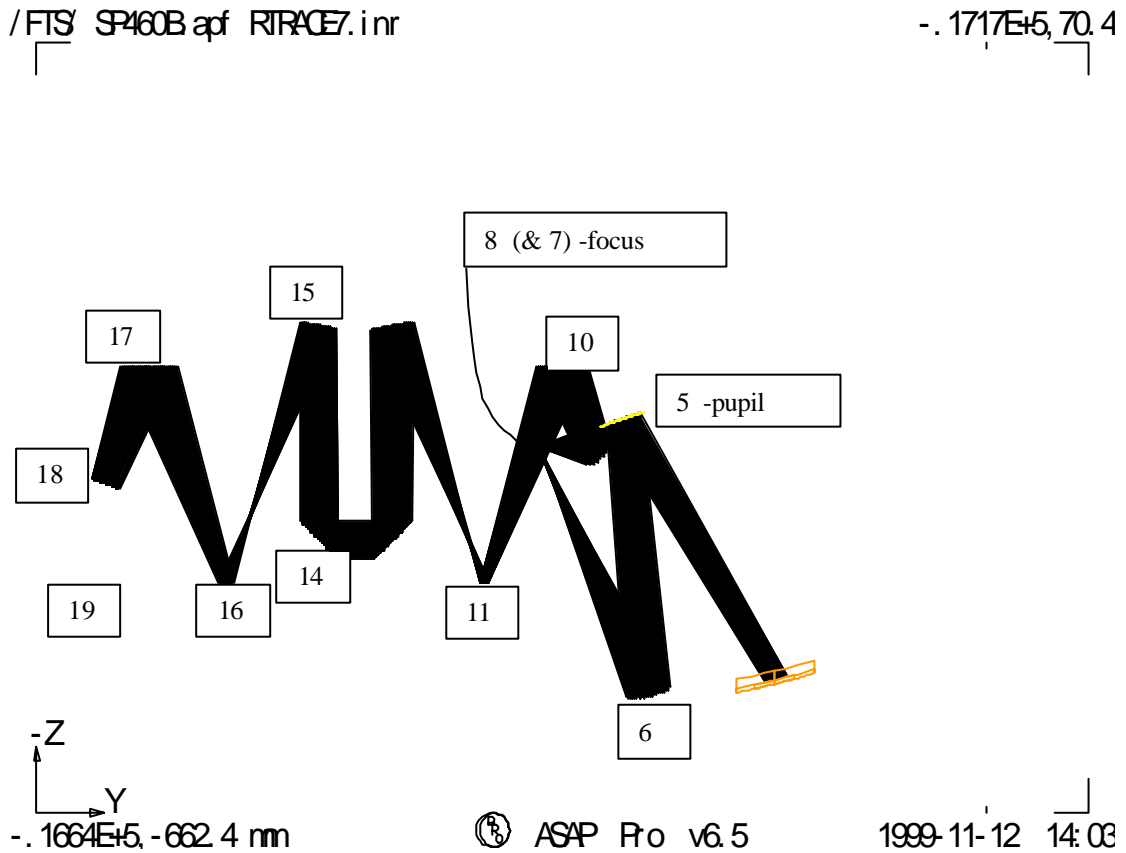
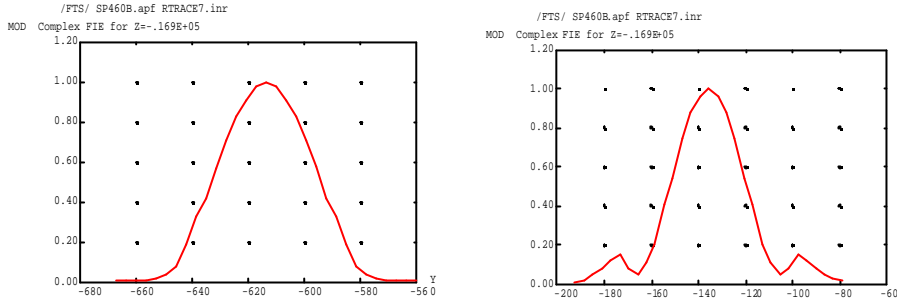


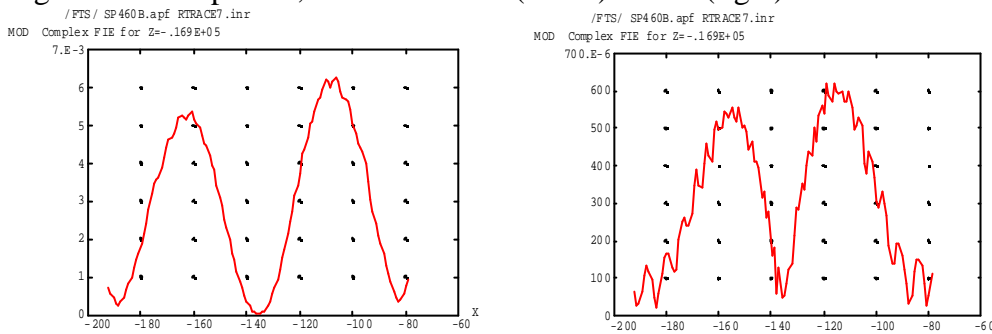
Fig.4. FTS model, sp460b.

2.1 Clipping at cold stop.

The beam is first clipped at the cold stop object #18. The beam pattern at this component is shown below.

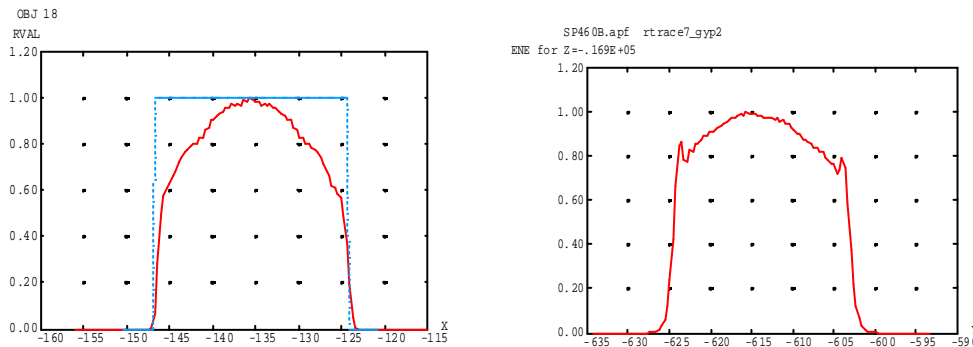


ASAP Pro v6.5 1999-11-11 17:29
Fig.5.a. Ex component, slices versus Y (at left) and X (right).



ASAP Pro v6.5 1999-11-11 17:45
Fig.5.b. Ey component, slices in direction of maximum (45 degree from X) at left, and parallel to X (right), where magnitude is much lower.

N.B. the relative magnitudes of the peaks in Ex & Ey are $E_x = 0.07$, $E_y = 0.006$.
 The cold stop aperture has diameter=22.6 mm (=45 wavelengths), so only a small portion at the centre of the beam is transmitted, as shown in fig.6. below. For Ey this has negligible flux (the 2 sidelobes are largely blocked) & so the Ey component is not propagated further.



ASAP Pro v6.5 1999-11-12 13:42
Fig.6. 'Ex' plots as per fig.5a, in Energy (intensity) & with cold-stop clipping applied.

The top-hat profile also plotted is to show the extent of the GO beam, which is in this case co-incident with the cold stop edge (chosen as circular, radius 11.3mm).

SPIRE	Technical Note	Ref: SPIRE-RAL- NOT-000316
	Beam patterns in FTS. 1. Long wavelength, lowest order mode.	Issue: 1 Date: 18-11-99 Page: 5 of 7

The 'spikes' in the plot at left are a numerical artefact. The limited sharpness of the aperture edge clipping is due to limited sampling of 31 points. (sample spacing > wavelength).

2.2 Efficiency.

This severe clipping by the cold stop will lead to low coupling efficiency of the mode to the energy collected by the telescope. This is understood to be a consequence of the detector horn (particularly its aperture size) being optimised for the higher-order modes at shorter wavelengths, and so being too small to work efficiently at this wavelength.

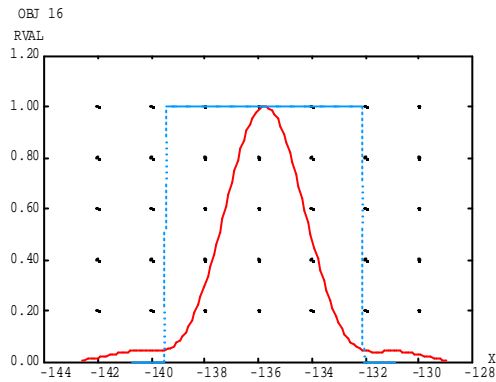
In this regard it is worth noting that to maximise the gain for given horn length ($L=30\text{mm}$ here), the diameter should be approx. $\sqrt{3\lambda L} = 6.7\text{mm}$, approx. twice the size which is used here (ref.1). This reference also notes that for maximum coupling the telescope beam should be presented to the horn aperture with top-hat shape, i.e. the pupil should be imaged to the horn aperture. This can only be done in non-imaging (i.e. single horn) systems, and it is again only possible for horn apertures many times larger in wavelength terms (e.g. in SPIRE the horn is just 7 wavelengths across at this wavelength whereas the system exit pupil is 45 wavelengths across).

For SPIRE we will need to calculate the reduced efficiency due to the presentation of the focused (Airy pattern-like) telescope beam at the horn aperture¹.

2.3 Rest of instrument.

The next series of plots shows the beam pattern slice versus X (ie perpendicular to symmetry plane) at some components of interest, in order of reverse propagation. Each plot includes the GO beam size as a top-hat profile, so that the diffractive spreading relative to GO can be seen.

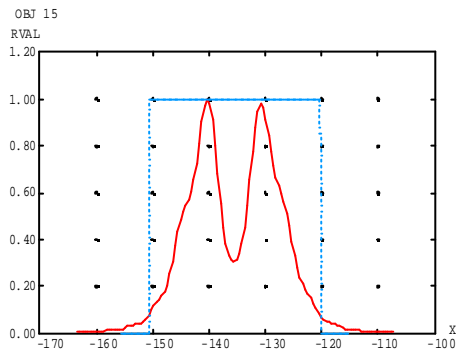
¹ This will be done by using a separate *forward* propagation model of the telescope top-hat beam, plus calculation of the coupling of this to each mode (at the horn aperture). In such a model the modes themselves will not need to be propagated. The same method can be simply extended to simulate the instrument PSF, as efficiency (across all modes) versus position of far-field point source.



ASAP Pro v6.5

1999-11-12 13:42

(a) At object #16, - beam combiner.

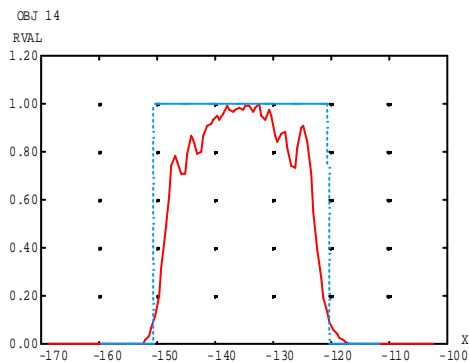


ASAP Pro v6.5

1999-11-12 13:42

(b) Object 15 , interferometer collimating mirror.

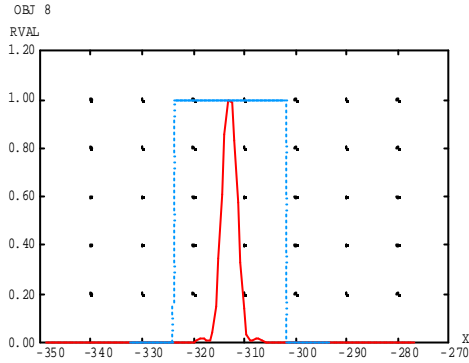
N.B. the wings of the beam are significant with respect to the limited size of these collimating mirrors.



ASAP Pro v6.5

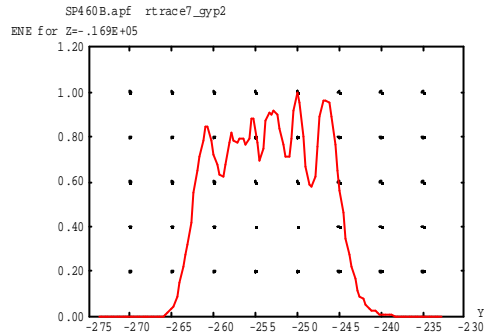
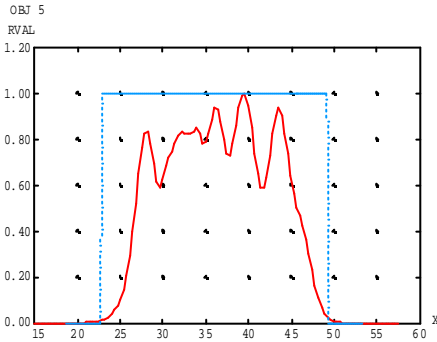
1999-11-12 13:42

(c) Object 14, mirror face of rooftop. N.B. this is close to a pupil plane, so the beam shape regains sharper edges and similarity to that at cold stop.



ASAP Pro v6.5 1999-11-12 13:42

(d) Object 8, Focal plane, pick-off mirror.



ASAP Pro v6.5 1999-11-12 14:24

ASAP Pro v6.5 1999-11-12 14:26

(e) Object 5. Chopper plane (pupil), in both slices.

N.B. At this point the numerical errors in the ray-set have built up to the non-paraxial ≈ 0.5 wavelengths level, so errors are present. To restore accuracy the beam will need to be re-decomposed ahead of this point. This will be included in the next version of this note.

The pupil-plane beam pattern at the chopper is also smaller than expected and is asymmetric. This may be due to the errors noted above, but is also likely to be due to the anamorphism of the optics which is not included here (input beam has circular cold-stop of $F=5$, whereas design has 20 % anamorphism). The actual size & shape for the cold stop is not well defined in the present design (due to pupil aberrations) and needs to be clarified for the next iteration.

The same model will next be used to propagate the other modes at the centre-wavelengths of each channel.

Ref.1. "Aperture efficiencies of large axi-symmetric reflector antennas fed by conical horns" J.A. Murphy. IEEE Trans. AP-Vol.36, No.4 (1988)